Journal of Materials Chemistry B

Accepted Manuscript

ROYAL SOCIETY OF CHEMISTRY

www.rsc.org/materialsB

Journal of Materials Chemistry B

Dynamic Article Links ►
View Article Online
DOI: 10.1039/C5TB00451A

Cite this: DOI: 10.1039/c0xx00000x

www.rsc.org/xxxxxx

ARTICLE TYPE

Decorating graphene oxide/nanogold with dextran-based polymer brushes for the construction of ultrasensitive electrochemical enzyme biosensors

Abderrahmane Boujakhrout,[a] Alfredo Sánchez,[a] Paula Díez,[a] Sandra Jimenez,[a] Paloma Martínez-Ruiz,[b] Miriam Peña-Álvarez,[c] José M. Pingarrón,*[a,d] Reynaldo Villalonga*[a,d]

Received (in XXX, XXX) Xth XXXXXXXXX 20XX, Accepted Xth XXXXXXXXX 20XX
DOI: 10.1039/b000000x

A novel strategy was employed to prepare a water-soluble graphene derivative by using dextran-based polymer brushes as solubilizing agents. Graphene oxide was grafted with (3-mercaptopropyl) trimethoxysilane and further decorated with Au nanoparticles. This hybrid nanomaterial was then reduced and anchored with polysaccharide-based polymer brushes by chemisorption of an end-group thiolated dextran derivative on the Au nanoparticles. The resulting hybrid nonmaterial allowed highly stable aqueous dispersions to be obtained, which were used to coat glassy carbon electrodes for the preparation of a model tyrosinase electrochemical biosensor for catechol. The enzyme electrode showed excellent electroanalytical performance with fast response in about 5 s, linear range of 100 pM – 120 nM, a very high sensitivity of 45.9 A/M and very low detection limit of 40 pM for catechol.

Introduction

The design of novel hybrid nanomaterials with well-defined and desired properties is a cornerstone for the development of advanced and miniaturized electronic devices, drug carrier systems and fuel and solar cells.[1] These advanced nanomaterials can be also employed as building blocks for the assembly of nanostructured surfaces for the construction of reliable and robust electrochemical biosensors.[2] For such analytical application, highly electroconductive nanomaterials with improved capability for the stable immobilization of biological receptors are mainly desired.

Since its discovery, graphene have emerged as a usefulness nanomaterial for electroanalysis,[3] due to the unique electroconductive properties, relative low cost, large surface-to-volume ratio, flexibility, remarkable mechanical and thermal stability and biocompatibility of this nanomaterial.[4] However, graphene is a highly hydrophobic nanomaterial showing very low solubility in water and many organic solvents, and tending to form irreversible agglomerates through strong π–π stacking and Van der Waals interactions.[5] In addition, the absence of chemical functional groups in graphene limits the stable and large immobilization of biomolecules through covalent linkages.[2a] For these reasons, the design of new graphene hybrid derivatives for biosensor technology has received considerable attention.

Graphene nanohybrids have been mainly prepared by chemical derivatization of either the raw nanomaterial or graphene oxide (GO),[6] a water soluble derivative that can be easily prepared by oxidative treatment of graphite.[7] However, these methods often yield nanomaterials with poor electroconductive characteristics due to the large destruction of the hyperconjugated π system in graphene, which reduces the electron mobility in the nanosized material. Recently we proposed the group-selective silanization of the hydroxyl groups on the basal planes of GO for further anchoring of polymeric materials as a useful approach to prepare soluble and highly functionalized graphene derivatives with low modification of its basal structure.[8]

A great variety of polymer-graphene nanohybrids have been described in literature.[9] In general, these materials showed high coverage of the carbon sheets with the macromolecules yielding derivatives with improved solubility and biocompatibility. However, such high surface coverage can limit the application of these nanohybrids in biosensors technology due to reduction of the electron and mass transfer processes at the electrode surface by steric hindrance. In this sense, we envision a novel solution for this nanomaterial engineering problem by site-selective and spaced low-degree modification of graphene nanomaterials and further anchoring of natural polymer brushes at such modification points.

Polymer brushes are long-chain polymer molecules attached by one end to a surface or interface with a relative high coverage density, and with the ability to produce a noticeable local change of the physic-chemical properties of such surfaces or interfaces.[10] Synthetic polymer brushes have been previously employed in biosensor design, demonstrating that their use can enhance the biosensor response by increasing the number of bioactive sites due to the high concentration of functional groups at the brush interface.[11] However, the design of a biosensor device using a nanohybrid modified with polysaccharide-based polymer brushes has not been described yet despite the well-known advantages associated with the use of such natural polymers in protein

View Article Online
DOI: 10.1039/C5TB00451A

immobilization and stabilization.[12]

In this work we describe, for the first time, the preparation of a novel water-soluble graphene derivative with polysaccharide brushes. The preparation of this nanohybrid was performed through the initial modification of GO with (3-mercaptopropyl) trimethoxysilane, using the hydroxyl groups at the basal plane as anchoring points. The silanized GO (Sil-GO) was then decorated with gold nanoparticles (Au-Sil-GO) and further reduced and anchored with polysaccharide-based polymer brushes by chemisorption of an end-group thiolated dextran derivative on the metal nanoparticles. The resulting hybrid nanomaterial (Dex-Au-Sil-rGO) was employed as transducer element for the design of a highly sensitive model electrochemical enzyme biosensor for cathecol. Although graphene/nanogold hybrid nanomaterials have been largely employed to construct electrochemical biosensors[13], to our knowledge, there are not previous reports dealing with the decoration of these nanohybrids with dextran brushes to yield a novel nanomaterial with improved characteristics for biosensor design and other purposes.

Materials and Methods

Materials

Tyrosinase (5370 U/mg), (3-mercaptopropyl) trimethoxysilane (MPTMS) and glutaraldehyde were acquired from Sigma-Aldrich Co. (USA). Dextran (4.5 kDa) was purchased from Serva Electrophoresis GmbH (Germany). Graphene oxide, prepared according to Hummers method,[14] was acquired from NanoInnova Technologies (Spain). All other chemicals were analytical grade.

Apparatus, electrodes and solutions

Amperometric measurements were performed with a dual-channel ultrasensitive Inbea potentiostat (Inbea Biosensores S.L., Spain). Cyclic voltammetry and electrochemical impedance spectroscopy experiments were performed using a FRA2 μAutolab Type III potentiostat/galvanostat (Metrohm Autolab B.V., The Netherlands). A conventional three-electrode system was employed in all electrochemical studies. The working electrode was a glassy carbon electrode (GCE, 3.0 mm diameter) modified with the graphene derivative and the immobilized enzyme. An Ag/AgCl/KCl (3 M) and a Pt wire were used as reference and counter electrodes, respectively. The measurements with the biosensor were carried out at 25ºC in 0.1 M sodium phosphate buffer, pH 6.0 (working volume 10 ml). Stock solutions of cathecol (100 nM, 1 μM and 10 μM) in 50 mM sodium phosphate buffer, pH 6.0, were freshly prepared.

The morphology of the nanohybrid was investigated using atomic force microscopy (AFM) with a SPM Nanoscope IIIa multimode microscope (Veeco Instruments Inc., USA). FT-IR spectra were acquired with a Nicolet Nexus 670/870 spectrometer (Thermo Fisher Scientific Inc., USA). Transmission electron microscopy (TEM) and high resolution transmission electron microscopy (HRTEM) measurements were performed with JEOL JEM-2000 FX and JEOL JEM-3000 F microscopes, respectively (Jeol Ltd., Japan). Power X-ray diffraction (XRD) was performed with an X'Pert MRD diffractometer (PANanalytical B.V., The Netherlands). Thermal analysis was performed with a TA Instruments SDT-Q600 apparatus (USA). High resolution field emission scanning electron microscopy (FE-SEM) was performed with a JEOL JSM-6335F microscope (JEOL Ltd., Japan).

Synthesis of end-group thiolated dextran

Monothiolated dextran derivative was synthesized by modification of our previous procedure.[15] Dextran (2 g), dissolved in 10 ml distilled water was mixed with 3.38 g cystamine hydrochloride and stirred during 2 h. 150 mg $NaCNBH_3$ was then added, and the reaction mixture was continuously stirred at room temperature overnight. $NaBH_4$ was then added up to 100 mM final concentration, and the mixture was stirred for 1 h. The solution was further extensively dialyzed vs distilled water using a Spectrapor 6 dialysis tubing (Serva, molecular weight cut-off 1000 Da) and finally lyophilized. The thiolated dextran derivative was characterized by ^{1}H-NMR spectrometry using a Bruker AV 500 MHz apparatus.

Synthesis of Dext-Au-Sil-rGO

Silanized graphene oxide was prepared by dispersion of 50 mg GO in 250 mL ethanol by sonication for 1 h. The dispersion was then heated at 65ºC, mixed with 25 mL of a 1% (v/v) ethanolic solution of MPTMS and kept under continuous stirring at this temperature during 12 h. The mixture was cooled and filtered and the resulting solid (Sil-GO) was exhaustively washed with ethanol and finally dried in vacuum over P_2O_5.

To prepare the Au-Sil-rGO derivative, 50 mg Sil-GO and 150 mg $NaBH_4$ were dispersed in 40 mL milliQ water by sonication and the dispersion was mixed with 20 mL citrate-capped Au nanoparticles (20 nm), prepared according to Frens procedure.[16] The solution was stirred at room temperature for 2 h, centrifuged and the solid was exhaustively washed with ethanol and dried under vacuum at room temperature.

Dex-Au-Sil-rGO was synthesized by dispersing 50 mg Au-Sil-GO in 50 mL milliQ water and further mixing with 500 mg end-group thiolated dextran. The mixture was stirred for 12 h at room temperature, then filtered and the solid was washed several times with ethanol and finally dried under vacuum at room temperature.

Preparation of the enzyme electrode

A bare GCE (3.0 mm diameter, electrochemical surface area = 6.99 mm^2) was first polished to mirror-like surface with alumina powder (0.3 μm), rinsed thoroughly with double distilled water, successively washed with double distilled water, anhydrous ethanol and acetone in an ultrasonic bath, and dried under N_2 before use. Coating of the polished GCE was accomplished by depositing two 10-μL aliquots of a 0.5 mg/mL Dex-Au-Sil-rGO aqueous dispersion on the electrode surface and allowing drying. Tyrosinase was immobilized on the modified electrode by dropping 20 μL of a 10 mg/mL enzyme solution in 100 mM sodium phosphate buffer, pH 6.0, and mixed with 4 μL of 25% (v/v) glutaraldehyde. The electrode was kept at 4ºC for 1 h, then washed several times with cold 50 mM sodium phosphate buffer, pH 6.0, and finally stored in refrigerator until use (Tyr/Dex-Au-Sil-rGO/GCE).

Journal of Materials Chemistry B
Dynamic Article Links ►
View Article Online
DOI: 10.1039/C5TB00451A
Cite this: DOI: 10.1039/c0xx00000x
www.rsc.org/xxxxxx
ARTICLE TYPE

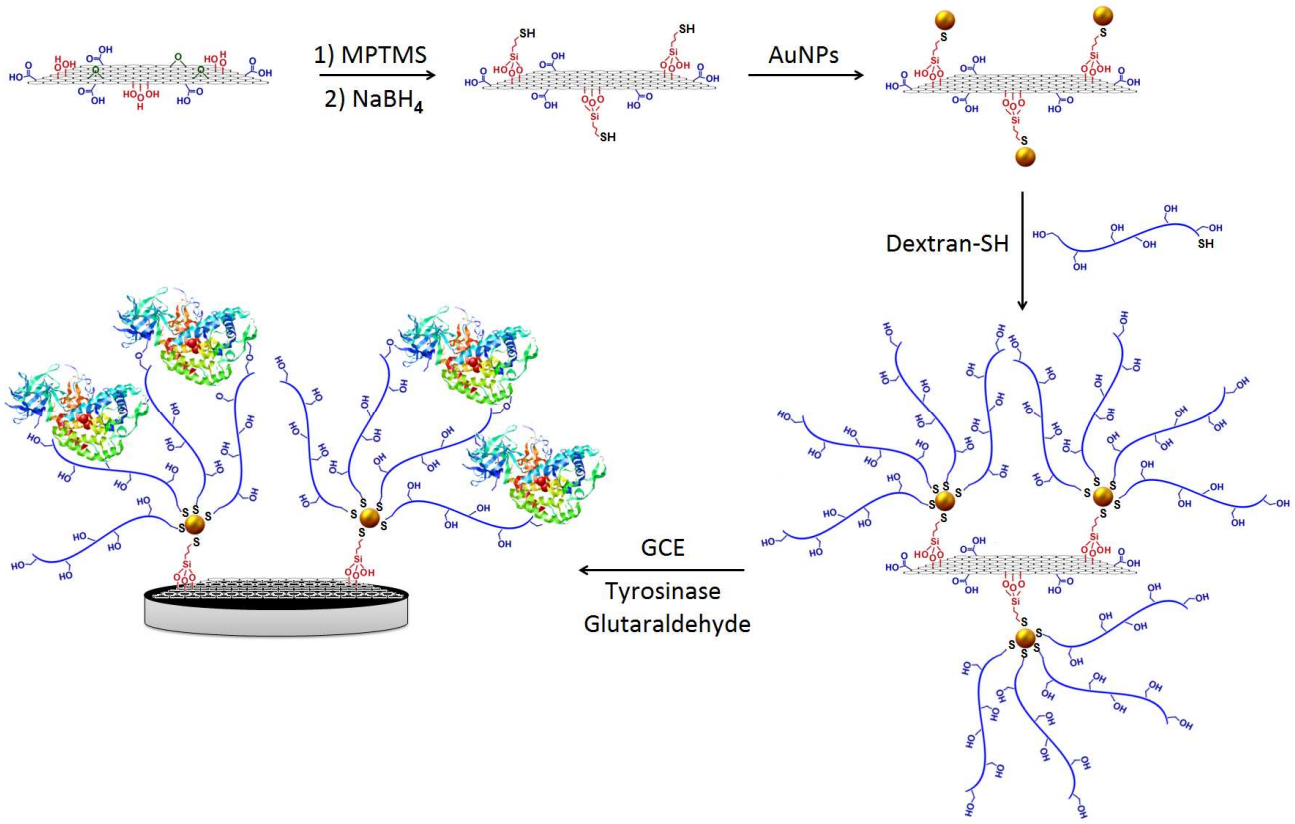

Fig. 1. Schematic display of the steps involved in the preparation of the Tyr/Dex-Au-Sil-rGO/GCE enzyme electrode.

Results and discussion

Figure 1 displays the different steps involved in the preparation of the nanohybrid and the further assembly of the sensing surface to construct the enzyme biosensor. Firstly, an end-group monothiolated dextran derivative was synthesized by reductive alkylation of low molecular weight dextran with cystamine in the presence of $NaCNBH_3$. Through this strategy, only the new imine bond formed at the reducing end of the polymer is reduced to a secondary amine group.

The modified dextran was further treated with $NaBH_4$ to disrupt the disulphide bond at the cystamine residue and then release the active thiol group. The successful preparation of such dextran derivative was confirmed by ^{1}H-NMR by the presence of a multiple signal at 2.15 ppm, corresponding to the methylene groups of the cysteamine residue at the end of the dextran derivative (Figure 1S in Supporting Information). The degree of polysaccharide modification was estimated as 87%, according to the ratio between the areas of the signals corresponding to the methylene groups of cysteamine and the anomeric protons at 4.87 ppm.

The graphene oxide nanohybrid was prepared through a three-step synthetic approach. In a first step, GO was enriched with reactive thiol groups by treatment with MPTMS, using the hydroxyl groups on the nanomaterial basal plane as anchoring points. Thiol-activated GO was then decorated with nanogolds by treatment with citrate-capped Au nanoparticles (AuNPs) in the presence of $NaBH_4$ to ensure reactivity of all -SH groups in the GO basal plane and to reduce GO. The metal surface of such nanoparticles was finally employed as modification points for the grafting of the end-group monothiolated dextran derivative through the formation of stable Au-S chemisorption linkages, yielding a dark product that was easily dispersed in aqueous solutions (Dex-Au-Sil-rGO). In fact, the nanohybrid material was easily dispersed in aqueous solutions up to a concentration of 1.3 mg/mL, the dispersions being stable for at least one month a room temperature.

Figure 2A shows the powder XRD analysis of the different graphene derivatives. GO showed an intense peak at 11.74º, corresponding to a *d*-spacing of about 7.54 Å. This interlayer distance can be ascribed to the presence of hydroxyl and epoxide groups on the basal planes and carbonyl and carboxyl groups at the sheet edges of GO, as well as the water molecules entrapped between the hydrophilic sheets.[17] Further modification of GO

View Article Online
DOI: 10.1039/C5TB00451A

with MPTMS, AuNPs and dextran decreased the intensity of this peak, which was also shifted to 11.48º (7.70 Å), 9.99º (8.85 Å) and 7.54º (11.71 Å), respectively. This increase in the interlayer distance could be ascribed to the bulky thiol groups, metal nanoparticles and polysaccharide brushes on the basal plane of GO. Diffractograms of Au-Sil-rGO and Dex-Au-Sil-rGO derivatives also showed peaks around 38.21º and 44.49º corresponding to (111) and (200) Bragg's reflection based on the fcc structure of gold nanoparticles.

Figure 2B shows Raman spectra of the graphene oxide derivatives. The spectrum of GO showed broad G and D bands at 1584 cm^{-1} and 1344 cm^{-1}, which characterize the in-phase vibration of the graphite lattice and the structural disorders at the graphite edges, respectively. These bands were only slightly shifted to 1588 cm^{-1} and 1347 cm^{-1} and the D/G intensity ratio remained unchanged (0.96) after modification with MPTS. However, the D/G intensity ratio significantly increased up to 1.10 in the Au-Sil-rGO and Dex-Au-Sil-rGO derivatives, suggesting a chemical interaction between the attached AuNPs and the graphene sheets. Similar enhancement in the D/G intensity ratio has been previously observed for other nanoparticles-graphene derivatives.[18] The attachment of AuNPs in the presence of $NaBH_4$ also caused a noticeable increase in the intensity of the 2D band around 2459 cm^{-1} for the Au-Sil-rGO and Dex-Au-Sil-rGO derivatives, which can be ascribed to the partial restacking of the graphene nanosheets after reductive treatment.[19]

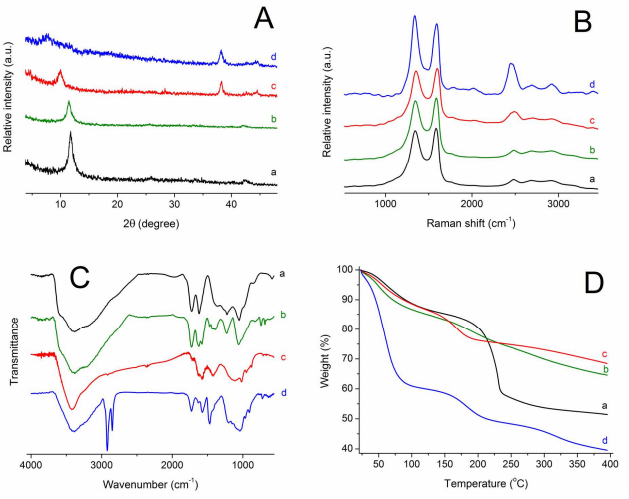

Fig. 2. A) X-ray diffraction, B) Raman spectroscopy, C) FT-IR and D) thermogravimetric, analysis of GO (a), Sil-GO (b), Au-Sil-rGO (c) and Dex-Au-Sil-rGO (d).

The FT-IR analysis of the graphene derivatives is shown in Figure 2C. GO exhibited sharp and broad peaks at 3607 cm^{-1} and 3090 cm^{-1} corresponding to the stretching of free and intermolecular H-bonded O-H groups, respectively. Moreover, the peaks at 1353 cm^{-1} and 1230 cm^{-1} can be ascribed to the stretching of C-OH and C-O-C groups in unoxidized graphitic domains of GO. The peaks at 1730 cm^{-1} and 1065 cm^{-1} in the GO spectrum can be associated to the stretching of the C=O and C-O groups, respectively. Finally, the peak at 1608 cm^{-1} could be ascribed to the vibrations of unoxidized graphitic skeletal domains as well as to the adsorbed water.[20]

The modification of GO with MPTMS was confirmed by the increased intensity of the peak at 1064 cm^{-1} due to the asymmetric Si-O-C stretching, as well as by the peak at 750 cm^{-1} associated to the bending of the Si-O-C groups. Although the attachment of AuNPs was not assessed by FT-IR, further grafting of the dextran brushes was confirmed by the broad peak centered at 3403 cm^{-1} due to the stretching of the O-H groups, the intense peaks at 2915 cm^{-1} and 2843 cm^{-1} corresponding to the stretching of the C-H groups, the O-H deformation peak at 1460 cm^{-1} and the C-O-C deformation peak at 1050 cm^{-1} in the FT-IR spectrum of the polysaccharide-modified graphene derivative.

The thermal stability of the graphene oxide derivatives was investigated by thermogravimetric analysis (Figure 2D). GO displayed two thermal decomposition processes in the range of 25-150ºC (ca. 14.3%) and 200-250ºC (ca. 30.7%), corresponding to the removal of residual water and degradation of the oxygen containing functional groups, respectively. Modification with MPTMS and AuNPs reduced the thermal stability of the nanomaterial by shifting the temperature for the maximum rate of weight loss from 231ºC to 188ºC and 169ºC, respectively. However, a noticeable reduction in the thermal weight loss of GO was observed after such modifications.

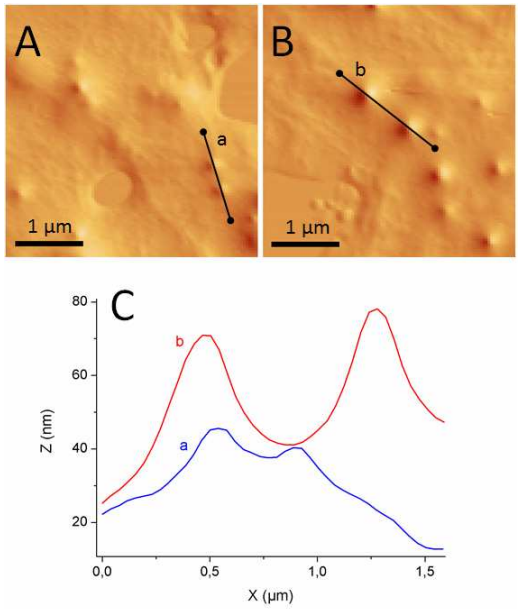

Fig. 3. AFM analysis for Au-Sil-rGO (A) and Dex-Au-Sil-rGO (B). C) Section analysis for Au-Sil-rGO (a) and Dex-Au-Sil-rGO (b).

Further attachment of the dextran brushes at the AuNPs surface resulted in a different thermogravimetric pattern with three well-defined thermal decomposition processes. This hybrid nanomaterial exhibited a remarkable weight loss of about 40% at temperatures up to ca. 100ºC, which was attributed to the thermodesorption of physically adsorbed water molecules. This high content of residual water can be justified by the high hydrophilicity of the polysaccharide. A second thermal-induced transformation, with maximum rate of weight loss at about 187ºC and a mass removal of about 10.6% was observed, which could be associated with the decomposition of the remaining carboxylate groups at the reduced GO edges. The dextran-

View Article Online
DOI: 10.1039/C5TB00451A

modified nanohybrid showed a third decomposition step in the range of 290-380ºC which is attributable to the degradation of the polysaccharide. According to thermogravimetric analysis, the content of dextran in the Dex-Au-Sil-rGO hybrid nanomaterial was estimated as 10.4% in weight.

Topological analysis of the nanohybrid was performed by AFM (Figure 3). AuNPs were clearly observed on the surface of Au-Sil-rGO and Dex-Au-Sil-rGO derivatives. However, a noticeable 3.9-fold increase in the thickness of AuNPs was observed after surface modification with the polysaccharide, as revealed by the AFM profiles. This fact suggested a high density of polysaccharide molecules attached to the surface of the metal nanoparticles, then producing a large extension of the dextran chains in a brush-type pattern and resulting in an unusual size increase of the modified nanoparticles.

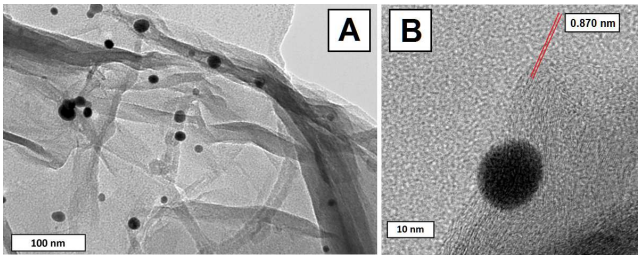

Fig. 4. TEM and HRTEM images Dex-Au-Sil-rGO.

Figure 4 shows representative TEM and HRTEM images of the Dex-Au-Sil-rGO nanohybrid. This analysis also confirmed the presence of AuNPs on the graphene surface. As it can be also observed in the FE-SEM image (Figure 5), a low density of AuNPs, homogenously distributed on the graphene basal plane, appeared attached to the carbon nanomaterial. This fact confirmed the successful preparation of a graphene nanohybrid with improved solubility properties through a minimum modification of the carbon nanostructure.

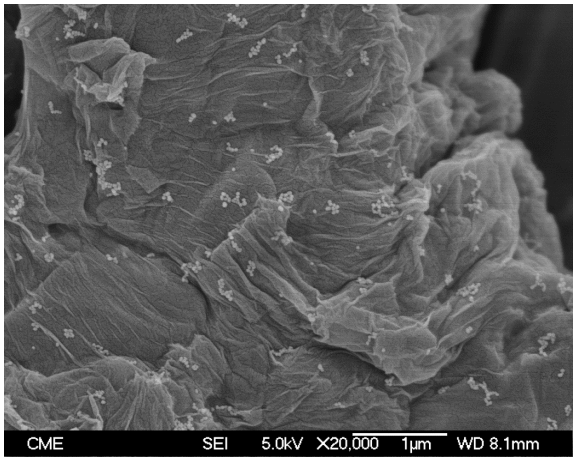

Fig. 5. FE-SEM image of Dex-Au-Sil-rGO.

HR-TEM images revealed that lattice fringes are visible on the edges of the Dex-Au-Sil-rGO nanohybrid due to sheets folding and/or rolling. The inter-layer spacing between neighbouring fringes was determined to be 0.870 nm, which is larger than the interplanar spacing in graphite (0.340 nm),[21] but slightly lower than that estimated by XRD. This higher inter-layer spacing can be justified by the presence of bulky AuNPs and dextran brushes on the basal plane of the reduced graphene oxide sheets.

The hybrid nanomaterial was evaluated as a transducer scaffold for the design of an electrochemical enzyme biosensor for catechol. As it is illustrated in Figure 1, the biosensor was assembled by coating glassy carbon electrodes with the Dex-Au-Sil-rGO hybrid nanomaterial and further immobilization of the enzyme tyrosinase by cross-linking with glutaraldehyde on the polysaccharide brushes. The conditions for the assembly of the Tyr/Dex-Au-Sil-rGO/GCE electrodes were optimized by evaluating the influence of different parameters on the amperometric signal of the biosensor. Larger analytical responses were achieved by coating the electrodes with 10 µg of nanohybrid and immobilization of 200 µg tyrosinase by using 4% (v/v) glutaraldehyde.

The assembly of the electrode under such optimal conditions was studied by electrochemical impedance spectroscopy using $[Fe(CN)_6]^{4-/3-}$ as redox probe (Figure 2S in Supporting Information). All the experimental data were obtained by fitting with a conventional Randles equivalent circuit. Functionalization of the electrode surface with the hybrid nanomaterial significantly reduced the electron transfer resistance of the interface (from R_{et} = 253 Ω to R_{et} = 64 Ω). This finding suggests high conductivity properties for the graphene/nanogold hybrid material, then favouring the fast occurrence of the electron transfer processes at the surface of the nanohybrid modified electrode. On the contrary, a large increase in the R_{et} value, 471 Ω, was apparent after the covalent immobilization of the enzyme indicating the successful attachment of the protein molecules.

These results were confirmed by cyclic voltammentry in the same working solution for the different electrode architectures (data not shown). By using the Randles-Sevcik model, the electrochemical surface area of the GCE was estimated to change from 7.1 mm^2 to 9.7 mm^2 and 14.1 mm^2 after sequential modification with SWNT and electropolymerized Au nanoparticles, respectively.

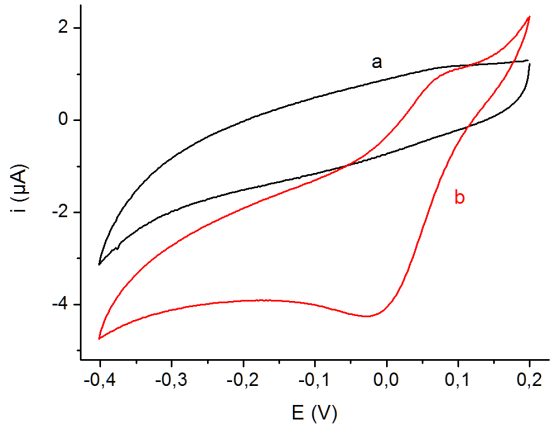

Fig. 6. Cyclic voltammograms recorded at the Tyr/Dex-Au-Sil-rGO/GCE in 0.1 M sodium phosphate buffer, pH 6.0 at scan rate of 50 mV/s before (a) and after addition of 10 nM (b) catechol.

The behaviour of the Tyr/Dex-Au-Sil-rGO/GCE as an enzyme electrode was checked by cyclic voltammetry using cathecol as a model substrate. As can be observed in Figure 6, a noticeable electroanalytical signal corresponding to the electrochemical reduction of the 1,2-benzoquinone formed through the enzyme-catalyzed reaction, was generated at a remarkable low

View Article Online
DOI: 10.1039/C5TB00451A

concentration level of 10 nM. Accordingly, the nanostructured enzyme electrode was further evaluated to construct an amperometric biosensor for this analyte.

The operational conditions for the amperometric detection of catechol were optimized, revealing that higher amperometric signals were achieved when the working potential was fixed at -100 mV *vs* Ag/AgCl, and the measurements were performed at pH 7.0.

The enzyme biosensor constructed with this nanohybrid modified electrode showed excellent an electroanalytical performance for catechol. Figure 7 shows the amperometric responses of the biosensor upon continuous addition of the analyte. The biosensor exhibited fast response, reaching 95% of the steady-state current within 5 seconds after the addition of catechol. The measured steady state current showed a linear dependence with catechol concentration over a large range, 100 pM to 120 nM (r = 0.9995), according to the following equation:

$$i_c(\text{A}) = 45.9\times\text{c(cathecol/M)} - 6.0\times10^{-9}$$

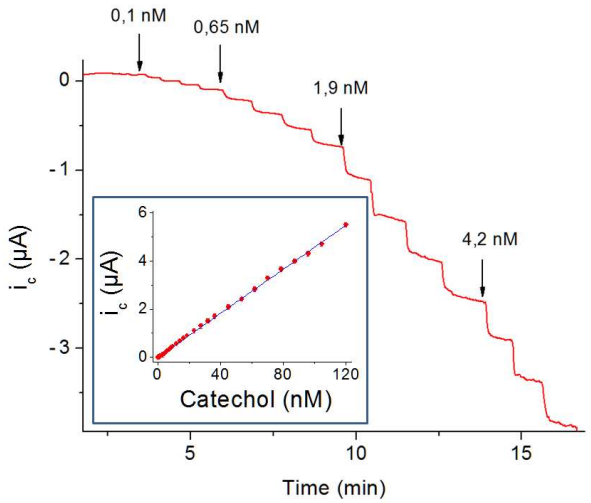

Fig. 7. Amperometric response of the biosensor for different catechol concentrations. Inset: Calibration curve. E_{app} = - 100 mV.

This relative narrow linear range of response (three order of magnitude) could be attributed to the high sensitivity achieved with the enzyme electrode, in agreement with previous reports describing this general behaviour for electrochemical sensors and biosensors.[22] In the present work, the nanostructured biosensor exhibited a very high sensitivity of 45.9 A/M (656 A/M cm^2), and a very low detection limit of 40 pM. These analytical characteristics are, by far, better than those previously reported for other tyrosinase biosensors based on graphene derivatives (Table 1S in Supporting Information), suggesting the excellent behaviour of the prepared nanohybrid for the immobilization of protein bioreceptors with electroanalytical purposes.

The apparent kinetics constants for the tyrosinase-mediated catalytic transformation of cathecol were determined as K_M = 5.7 μM and I_{MAX} = 26.0 μA (372 μA/cm^2). The apparent K_M value was over 42-fold lower than that reported for the free enzyme (240 μM).[23] This fact could be ascribed either to an increase in the affinity of the enzyme for the substrate or to the reduction of the effective value of V_{MAX} (k_{cat}) for the enzyme upon immobilization.

The selectivity of the biosensor was evaluated by measuring the amperometric response towards 2.5 nM catechol in the presence of five potential interfering substances at a 25 nM concentration level: bisphenol A, 4-tert-butylphenol, 17β-estradiol, 17α-ethinyl estradiol and hydroquinone. The biosensor exhibited an excellent selectivity towards catechol, and its amperometric response was only affected (~ 24%) by the presence of hydroquinone at this high concentration.

The reproducibility of the biosensor was estimated to be 8.1% by measuring the response of ten different electrodes to the same 10 nM catechol concentration. On the other hand, a repeatability of 5.8% was determined by using the same nanostructured electrode toward 10 different additions of the analyte at 10 nM final concentration. The enzyme biosensor also showed good stability upon storage at 4ºC under dry conditions, retaining full electroanalytical properties after 1 week of storage (Figure 3S in Supporting Information). At longer times of storage, the enzyme electrode suffered a progressive loss of activity, retaining over 58% of the initial activity after 2 weeks at 4ºC.

Conclusions

Here we described for the first time the preparation of a polysaccharide brushes-modified graphene oxide derivative. This novel hybrid nanomaterial was prepared by decorating a MPTMS-modified GO with AuNPs and further grafting of dextran brushes on the nanoparticles surface. The structural, morphological and electroconductive properties of this nanohybrid were characterized by using different techniques. This graphene derivative demonstrated its usefulness as electrochemical transducer for the design of an amperometric enzyme biosensor for catechol, which exhibited excellent analytical performance in terms of high sensitivity and low detection limit. These results suggest that decoration of graphene derivatives with polysaccharide-based polymer brushes offers new possibilities for the design of advanced hybrid nanomaterials for bio-electroanalytical purposes.

Acknowledgements

R. Villalonga acknowledge to Ramón & Cajal contract from the Spanish Ministry of Science and Innovation. Financial support from the Spanish Ministerio de Ciencia e Innovación CTQ2011-24355, CTQ2012-34238 and Comunidad de Madrid S2013/MIT-3029, Programme NANOAVANSENS is gratefully acknowledged.

Notes and references

[a]*Department of Analytical Chemistry,* [b]*Department of Organic Chemistry I &* [c]*Department of Physical Chemistry I, Faculty of Chemistry, Complutense University of Madrid, 28040-Madrid Spain. Fax: +34 913944329; Tel: +34 913944315;*
E-mail: pingarro@quim.ucm.es, rvillalonga@quim.ucm.es

† Electronic supplementary information (ESI) available: Characterization of the hybrid nanomaterial and the enzyme biosensor.

1 a) K.M. Taylor-Pashow, J. Della Rocca, R.C. Huxford, W. Lin, *Chem. Commun.*, 2010, **46**, 5832; b) P. Díez, A. Sánchez, M. Gamella, P. Martínez-Ruíz, E. Aznar, C. de la Torre, J.R. Murguía, R. Martínez-Máñez, R. Villalonga, J.M. Pingarrón, *J. Am. Chem. Soc.*, 2014, **136,** 9116; c) A. Mehdi, C. Reye, R. Corriu, *Chem. Soc. Rev.*, 2011, **40**, 563; d) R. Villalonga, P. Díez, A. Sánchez, E. Aznar, R. Martínez-Máñez, J.M. Pingarrón, *Chem. Eur. J.*, 2013, **19**, 7889.

View Article Online
DOI: 10.1039/C5TB00451A

2 a) Y. Liu, X. Dong, P. Chen, *Chem. Soc. Rev.*, 2012, **41**, 2283; b) R. Villalonga, P. Díez, S. Casado, M. Eguílaz, P. Yáñez-Sedeño, J.M. Pingarrón, *Analyst*, 2012, **137**, 342; c) R. Villalonga, P. Díez, P. Yáñez-Sedeño, J.M. Pingarrón, *Electrochim. Acta*, 2011, **56**, 4672; d) M. Martín, P. Salazar, R. Villalonga, S. Campuzano, J.M. Pingarrón, J.L. González-Mora, *J. Mat. Chem. B*, 2014, **2**, 739; e) R. Villalonga, C. Camacho, R. Cao, J. Hernández, J.C. Matías, *Chem. Commun.,* 2007, 942; f) R. Villalonga, P. Díez, M. Eguílaz, P. Martínez, J.M. Pingarrón, *ACS Appl. Mater. Interfaces*, 2012, **4**, 4312.

3 a) F. Xiao, Y. Li, X. Zan, K. Liao, R. Xu, H. Duan, *Adv. Funct. Mat.*, 2012, **22**, 2487; b) E. Araque, C.B. Arenas, M. Gamella, J. Reviejo, R. Villalonga, J.M. Pingarrón, *J. Electroanal. Chem.*, 2014, **717-718**, 96; c) E. Araque, R. Villalonga, M. Gamella, P. Martínez-Ruiz, A. Sánchez, V. García-Baonza, J.M. Pingarrón, *ChemPlusChem*, 2014, **79**, 1334.

4 M.J. Allen, V.C. Tung, R.B. Kaner, *Chem. Rev.*, 2010, **110**, 132.

5 X. Yang, J. Zhu, L. Qiu, D. Li, *Adv. Mat.,* 2011, **23**, 2833.

6 a) H. Yin, C. Zhang, F. Liu, Y. Hou, *Adv. Funct. Mater.*, 2014, **24**, 2929; b) L. Li, G. Zhou, Z. Weng, X.Y. Shan, F. Li, H.M. Cheng, *Carbon*, 2014, **67**, 500.

7 D.R. Dreyer, S. Park, C.W. Bielawski, R.S. Ruoff, *Chem. Soc. Rev.*, 2010, **39**, 228.

8 E. Araque, R. Villalonga, M. Gamella, P. Martínez-Ruiz, J. Reviejo, J.M. Pingarrón, *J. Mat. Chem. B*, 2013, **1**, 2289.

9 a) A.Y. Sham, S.M. Notley, *Soft Matter*, 2013, **9**, 6645; b) K.E. Byun, D.S. Choi, E. Kim, D.H. Seo, H. Yang, S. Seo, S. Hong, *ACS Nano*, 2011, **5**, 8656; c) Y. Tang, N. Wu, S. Luo, C. Liu, K. Wang, L. Chen, *Macromol. Rapid Commun.*, 2012, **33**, 1780.

10 a) S.T. Milner, *Science*, 1991, **251**, 905; b) T. Chen, I. Amin, R. Jordan, *Chem. Soc. Rev.*, 2012, **41**, 3280; c) J. M. Bak, T. Lee, E. Seo, Y. Lee, H.M. Jeong, B.S. Kim, H.I. Lee, *Polymer*, 2012, **53**, 316.

11 a) M. Welch, A. Rastogi, C. Ober, *Soft Matter*, 2011, **7**, 297; b) T.R. Antonio, M.F. Cabral, I. Cesarino, S.A. Machado, V.A. Pedrosa, *Electrochem. Commun.*, 2013, **29**, 41; c) Z.B. Zhang, S.J. Yuan, X.L. Zhu, K.G. Neoh, E.T. Kang, *Biosens. Bioelectron.*, 2010, **25**, 1102.

12 a) M.L. Villalonga, P. Díez, A. Sánchez, M. Gamella, J.M. Pingarrón, R. Villalonga, *Chem. Rev.*, 2014, **114**, 4868; b) L. Gómez, H. L. Ramírez, M. L. Villalonga, J. Hernández, R. Villalonga, *Enzyme Microb. Technol.*, 2006, **38**, 22; c) A. Valdivia, R. Villalonga, M. G. Sommella, Y. Pérez, L. Mariniello, R. Porta, *J. Biotechnol.*, 2006, **122,** 326; d) R. Darias, I. Herrera, A. Fragoso, R. Cao, R. Villalonga, *Biotechnol. Lett.*, 2002, **24**, 1665; e) A. Valdivia, Y. Perez, A. Dominguez, J. Caballero, L. Gomez, E. H. Schacht, R. Villalonga, *Macromol. Biosci.,* 2005, **5,** 118.

13 a) D. Pan, Y. Gu, H. Lan, Y. Sun, H. Gao, *Anal. Chim. Acta*, 2015, **853**, 297; b) Y. Yu, Z. Chen, S. He, B. Zhang, X. Li, M. Yao, *Biosens. Bioelectron.*, 2014, **52**, 147; c) Y. Yang, A.M. Asiri, D. Du, Y. Lin, *Analyst*, 2014, **139**, 3055.

14 W.S. Hummers, R.E. Offeman, *J. Am. Chem. Soc.,* 1958, **80**, 1339.

15 a) Y. Pérez, A. Valdivia, L. Gómez, B. K. Simpson, R. Villalonga, *Macromol. Biosci.*, 2005*,* **5,** 1220; b) R. Villalonga, S. Tachibana, Y. Pérez, Y. Asano, *Biotechnol. Lett.*, 2005, **27**, 1311.

16 G. Frens, *Nature*, 1973, **241**, 20.

17 S. Park, J. An, I. Jung, R.D. Piner, S.J. An, X. Li, A. Velamakanni, R.S. Ruoff, *Nano Letters,* 2009, **9**, 1593.

18 a) A.R. Siamaki, A.E.R.S. Khder, V. Abdelsayed, M.S. El-Shall, B.F. Gupton, *J. Catal.*, 2011, 279, 1; b) K.S. Subrahmanyam, A.K. Manna, S.K. Pati, C.N.R. Rao, *Chem. Phys. Lett.*, 2010, **497**, 70.

19 Y. Hao, Y. Wang, L. Wang, Z. Ni, Z. Wang, R. Wang, C.K. Koo, Z. Shen, J.T. Thong, *Small*, 2010, **6**, 195.

20 J.F. Shen, Y.Z. Hu, M. Shi, X. Lu, C. Qin, C. Li, M.G. Ye, *Chem. Mater.,* 2009, **21**, 3514.

21 G. Lu, S. Mao, S. Park, R.S. Ruoff, J. Chen, *Nano Res.*, 2009, **2**, 192.

22 a) J.B. Raoof, R. Ojani, H. Karimi-Maleh, M.R. Hajmohamadi, P. Biparva, *Anal. Methods*, 2011, **3**, 2637; b) M.E. Ghica, C.M. Brett, *Anal. Lett.*, 2013, **46**, 1379.

23 J.L. Smith, R.C. Krueger, *J. Biol. Chem.,* 1962, **237**, 1121.

View Article Online
DOI: 10.1039/C5TB00451A

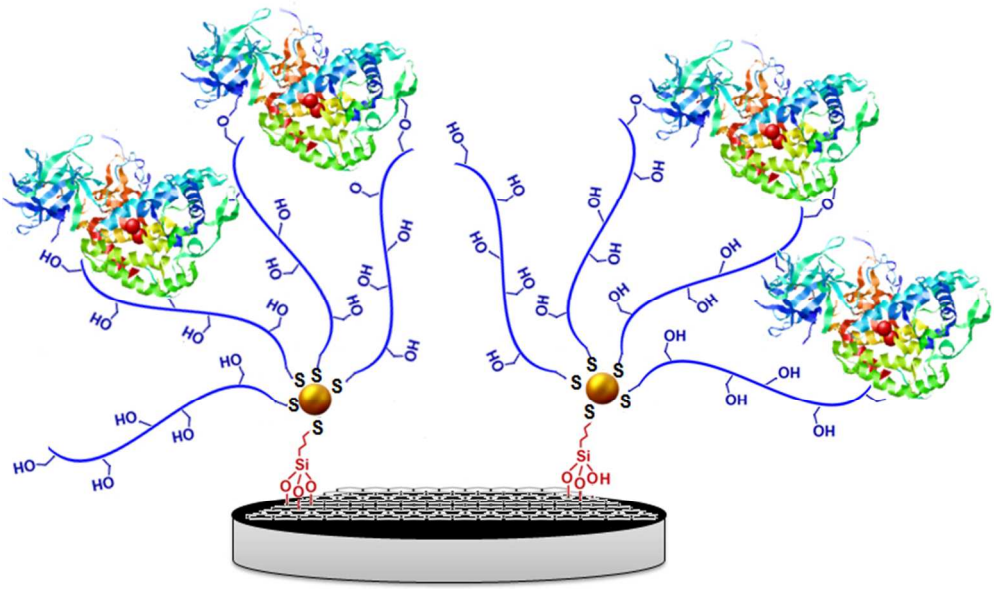

220x132mm (96 x 96 DPI)